Chapter 24

Experiments with Pneumatically-Formed Metalized Polyester Mirrors

Bruce D. Holenstein[1], Richard J. Mitchell[1], Dylan R. Holenstein[1], Kevin A. Iott[2] and Robert H. Koch[3]

[1]Gravic, Inc., Malvern, PA; [2]Iott Precision Instruments, Petersburg, MI; [3]Department of Physics and Astronomy,University of Pennsylvania, Philadelphia

Introduction

In a contribution earlier in this volume (Holenstein, Mitchell, & Koch 2010) (HMK), some of us presented an analysis for quantifying the imperfections of unconventional optical systems and correcting for them. Our primary motivation is credible and reproducible astronomical observational work and not lab applications. In this presentation, we lay out our developmental efforts toward that intended purpose and apply some of the earlier results to our developments and accomplishments since 1991.

Background

In 1991 Peter Waddell visited the Laboratory for Research on the Structure of Matter (LRSM) at the University of Pennsylvania. A member of the Department of Mechanical and Process Engineering of the University of Strathclyde, Glasgow, UK, Waddell delivered a lecture about John Logie Baird (1888-1946) and his sadly neglected (according to at least some Scots) claim to be the inventor of television. Waddell's baggage included an 8 inch pneumatic mirror which he drew into a focusing figure by sucking on a plastic tube and co-author Robert Koch witnessed the image of an outside scene displayed on an office wall with this device. Some results and interpretations from Strathclyde had already appeared in, e.g., King et al. (1985), and Manly (1991) has reviewed a part of Waddell's results. Gavin (1979), a British amateur astronomer, briefly reports on and illustrates a pneumatic telescope that he had designed and constructed.

The imaging stunt was reported to Kenneth Lande, then Chairman of Astronomy and Astrophysics, who authorized spending limited departmental funds to investigate the theory and realization of like mirrors. Over the next 5 years, a few people participated in fabrication and tests of them: Robert Hee as professional machinist and the late Samuel

The Alt-Az Initiative: Telescope, Mirror, & Instrument Developments. 2010. Genet, Johnson, & Wallen, eds.

Seeleman and Robert Koch as amateur ones and opticians; Richard Mitchell as hardware and electronics specialist; and an assortment of graduate students. Effort was dedicated to design, construction, and testing of 3 pneumatic imaging systems, and a few in-house demos and talks were given about them. Robert Koch visited the Waddell lab in 1994 studying a 24 in pneumatic mirror that had been kept under a substantial pressure difference for more than a year and, to visual inspection, preserved a good figure. Robert Koch's retirement in 1996 brought the opportunity to try a different design which he pursued until about 2000. Work on the project was re-engaged in 2008 when Bruce Holenstein pulled together the surviving collaborators to start anew, bringing Kevin Iott on board as designer and machinist and Dylan Holenstein as lab technician.

Hardware In Summary

There follows a summary of the items and processes that we have experimented with:

Reflecting materials: 0.2, 0.4, 0.6, 1.5, 1.7, 2.0, 4.5, 6.3, 6.8, and 7.2 mil aluminized or silvered polyester films (either one- or two-sided metalizing), some of which were Mylar® marketed under different brand names from U.S. manufacturers; 1 mil stainless steel shimstock.

Structural materials: 7-ply, 0.75 inch sealed marine plywood; 0.75 inch primed, painted, and sealed oak; 0.25 inch aluminum; 0.25 and 1.00 inch acrylic.

Retaining and clamping materials: threaded acrylic with O-rings; aluminum standoff posts with O-rings; hot-melt glue with cellular foam; discrete clamped spreader bars with cellular foam; bolted aluminum ring cells; rolled and welded aluminum sheet.

Optical diameters: 2 each 7.25 inch; 8 inch; 2 each 12 inch; 2 each 42 inch; and 70 inch.

Focal ratios: *f*/0.5 – *f*/10.

Pressure differences with respect to atmospheric: positive in a bladder with a transparent film or acrylic window; negative without a transparent window.

Pressure difference control: mouth; hand pump; electrical vacuum/pressure pump; laptop control of mini-valves.

The reader should not imagine that all combinations of these characteristics were tried experimentally nor should one suppose that the chronology of change has been monotonically from small to large or from naïve to complex. The reader will also notice in the following a mixture of metric and English units according to the measuring devices that we actually used.

Motivation

World-wide there have been several investigators of deformable optics and a certain number of them (including Waddell's radiant heating of some hardware for a bench experiment) had non-astronomical purposes in mind for their designs. Until very recently, we had not looked at the patent literature but were content to be guided by our own efforts. Our review of that literature does not indicate that we have significantly duplicated earlier work.

The ultimate purpose of our efforts has been to develop a pneumatic mirror that would be useful for astronomical photometric programs with a feedback control against ambient changes so as to sustain a constant focal length. A mirror surface that will satisfy our observing program will collect photons from a stellar program object and deliver them to the detector surface, yet exclude enough background photons in order to yield an acceptable signal-to-noise ratio.

Test Results

In the following we summarize our experience with significant features of our devices:

Film Stability

The film thicknesses given above are nominal and we did not make enough measures to determine the uniformity of thickness over an extended area of any sample. Thickness of the metalizing layers ranged from about 0.2 mil to about 1.2 mil but this too was not tested extensively.

No matter what the film thickness and no matter the manufacturer, reflecting film can be degraded easily as it is peeled from a roll. The width of our rolls was typically 48 inches but wider dimensions can be bought up to at least 12 feet. Unless film is restrained as the roll is unwound and unless the metalized surface is protected from abrasion, linear, curvilinear, or cornered folds are inevitable. The same care must be looked to when moving a cut film sample, for it may fold if caught in an airstream. Even with all precautions observed, an area of about 2 feet^2 or larger will not lie flat under its own weight as it comes off a roll; it will have obvious ripples with semi-amplitudes of the order of 0.125 inch.

At the LRSM we cycled a sample film from room temperature to -70 C a few times to see if a glass transition would occur in the film. No such transition happened in these repetitions. Eventually, the metal

and polymer delaminated, presumably because of the difference of the coefficients of thermal expansion.

Repeated cycling to a pressure differential of -0.5 inch of Hg and back to atmospheric led to an unchanged figure for the film and we were unable to detect any passing of the elastic limit. In order to look further at the elasticity of the film, we cut a sample 0.25 inch x 33.5 inch x 0.005 inch of 3M silvered film and loaded it statically along its long dimension with successively greater weights in a test that lasted 3 days. There were repeated changes, repetitions, and reversals of the loading during that interval. Over a considerable range of load the film performed according to:

$$Elongation = 0.006(4) - 0.000269(6)(\mathbf{Load}). \quad (1)$$

The parenthesized numbers (here as well as later) are the 1σ-errors of the last decimal place of the foregoing coefficients. This linear fit to the data shows that the sample elongated by about 0.4% up to (1200 gm < *Load* < 1500 gm). The result is consistent with the published elasticity of Mylar film and leads to a Young's modulus of 4 GPa, also consistent with the specs of the sample. Beyond a load of 1500 gm, elongation was faster.

Structural Materials

Because of pressure-difference losses, the oak frame needed many repetitions of interior and exterior fiberglass and epoxy sealing before all pores were sealed. None of the other materials suffered from this defect.

Retaining and Clamping Mechanisms

For a criterion of retaining a substantial pressure difference for many hours, the threaded 12 inch acrylic ring cell furnished with 0.125 inch O-rings and with contacting surfaces coated with stopcock grease would be considered adequate. (This device appears in Figure 2.) The small aluminum bolted cells were superior; they retained pressure differences of -5 inches of Hg against atmospheric for more than a month. The other mechanisms were failures. Insofar as discrete clamping points were used, their adjoining locations could not be separated more widely than about 1 inch on the cell circumference if ripple structure was to be invisible to the naked eye on the reflecting surface.

Control Against Ambient Changes

With an A. H. Thomas pump and a water manometer that we built, we could control the calibrated pressure difference to ±0.002 bar. The pump, with a capacity of 2 psi, moved 3.6 liters/minute and required of the order of 60 seconds to attain a good figure on the film mounted in a 12 inch cell. For film mounted in the 42 inch cells, pumping time was of the order of a few minutes using a Brey G12/02-8LC vacuum pump monitored with a Honeywell 142PC05D pressure sensor. There are numerous temperature and pressure sensors commercially available which can be suitably interfaced for computer control.

Figures and Focal Ratios

Early tests used a depth micrometer to determine gross figures for both of the 12 inch mirrors. These tests were run across a number of different diameters and corrected for the shape and size of the micrometer probe. One sample is shown in Figure 1. Polynomial curve-fitting to order 2 by the Levenberg-Marquart (L-M) method led to the representation of the figure:

$$y = 0.0003(7) + 0.0003(1)x + 0.00733(4)x^2 \quad (2)$$

The linear term is due to an asymmetry in mounting the film in the frame. Curve fitting to order 3 recovered the three coefficients above within their errors and showed the cubic term not to be significant. In principle, the quadratic term signifies an f/2.70 beam with a focus at F = 32.34 inch.

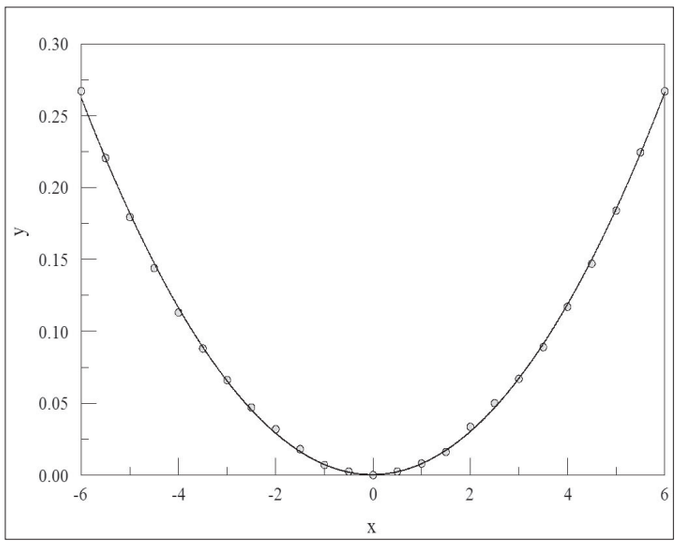

Figure 1: A mechanical determination, made in 1992, of the figure of a silvered Mylar membrane mounted in one of the 12 inch frames. The continuous curve is that of equation (2) of the text. A ripple structure can be seen from about |5.25| inch to about |1.5| inch.

However, as can be seen in the illustration, higher even-order terms are likely and curve fitting indeed established 4th- and 6th-order terms at close to the 3σ level. These fittings diminished the sum of the squared residuals by factors of 1.5 and 2.3, respectively, compared to the value found by the quadratic fit. The coefficients of the 4th- and 6th-order terms correspond to 9,140 Å and 2,290 Å, respectively, on the film surface. No matter whether this "fine" structure is confined to the sampled diameter or is limited to a circular sector or is circularly symmetric, it emphasizes the need for uniform tensioning of the film into a plane before the cell is closed. A tensioning frame must obviously be larger than the cell diameter.

Curve fitting, again by the L-M procedure, converged to a circular fit for a radius of 68.3(3) inches but with a sum of squared residuals about 20% worse than the simple parabolic fit.

There are published suggestions that the figure of a pressurized film is a catenary – the usual example being that of a cable restrained at its endpoints and hanging under its own weight. In a formal mathematical way, the L-M method cannot fit the data of Figure 1 by a catenary, but physically there is a more forceful reason why this geometry should not be suitable for a pressurized film. One lays aside, first of all, consideration of a textile string or rope, which characteristically has little weight and feels aerodynamical forces and, as an example, concentrates instead on a braided steel cable as an analogue to the pressurized film. This familiar element of a suspension bridge becomes configured as a catenary under its own mass but it lacks one characteristic of a pressurized film – the film deforms under the pressure difference because of its relatively large elasticity and this does not happen with construction steel. For this reason, further consideration of a catenary was considered unrealistic.

Our mechanical experiments, therefore, led us to believe that imaging defects would be traceable to zonal errors and classical astigmatism of the stretched film due to defects in tensioning, spherical aberration, and the bi-axial structure of the polymer itself.

Quickly thereafter and very recently as well, we ran numerous optical tests of figure by constructing the Right-angle Bath interferometer (mentioned above) fed by a He-Ne laser. The setup is

shown in Figure 2 with the beam aimed at a 1 mil aluminized film mounted in one of the 12 inch cells. The same figure also shows typical results for a 1 inch radius of the film (a choice made to keep the number of fringes to be analyzed reasonably small) offset by 4.5 inches from the center with a pressure difference of -5 inches of Hg against atmospheric.

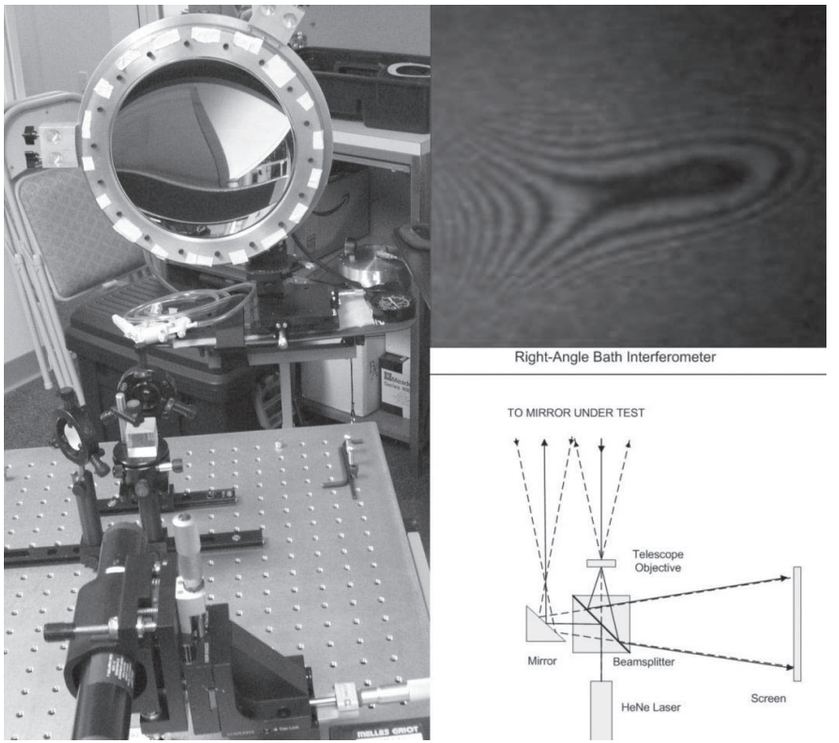

Figure 2: The tabletop optical bench mounting the interferometer, laser, and sample 12 inch film mirror, which is not under tension. The bolting pattern on the table is a 1 inch grid. In the lower right there is a schematic of the optical components and paths and above this sketch a sample interferogram.

Fitting of all interferograms was accomplished by *FringeXP* (Rowe 2003) and resulted in the sample Zernike coefficients listed in Table 1.

Table 1

Zernike Coefficients for Example Interferogram					
		(n,m)	**Coefficient**		**Type**
	Z_0	(0,0)	7.993		Piston
Z_1	Z_2	(1,1)	5.114	2.131	Tilt
	Z_3	(1,0)	2.147		Defocus (power)
Z_4	Z_5	(2,2)	-5.955	2.089	Astigmatism
Z_6	Z_7	(2,1)	0.9333	0.5471	Coma
	Z_8	(2,0)	-1.547		Principal Spherical
Z_9	Z_{10}	(3,3)	-0.9508	-0.08976	Trefoil
Z_{11}	Z_{12}	(3,2)	4.443	-2.009	Secondary Astigmatism
Z_{13}	Z_{14}	(3,1)	-1.305	-0.3269	Secondary Coma
	Z_{15}	(3,0)	0.1612		Secondary Spherical
Z_{16}	Z_{17}	(4,4)	-2.242	2.23	Tetrafoil
Z_{18}	Z_{19}	(4,3)	0.09358	-0.304	Secondary Trefoil
	Z_{21}	(4,2)	0.4233	-0.2649	Tertiary Astigmatism
Z_{22}	Z_{23}	(4,1)	-0.4218	-0.3383	Tertiary Coma
	Z_{24}	(4,0)	0.1182		Tertiary Spherical
					RMS fit Error: 0.05889 waves

The first three terms (piston, tilt, and defocus) are not related to the mirror figure for interferograms centered on the mirror. For off-axis interferograms, the terms must be understood as offsets from the values derived on centered and neighboring (partially overlapping) interferograms and must be used in a mirror analysis. Column 3 gives the conventional notation for the coefficients and columns 4 and 5 the fitting evaluations in waves. Terms 4 and higher are characterized simply by a large degree of astigmatism caused by the Young's modulus of

Mylar being bi-axial by about 5%, where the axes are along the rolling machine direction and in the transverse direction, and by our lack of tensioning control. This condition may be reduced markedly in future cells provided with mechanical or electrical control elements. The test configuration itself introduced about one wave of astigmatism because the right-angle Bath interferometer is not a common path interferometer. This instrumental astigmatism can be easily reduced by moving the right angle mirror closer to the beamsplitter. The tetrafoil aberration is due to the mutually-opposing four bolts that in this particular experiment were the first ones secured on the membrane clamp ring, again a detail that may be easily corrected.

Contour and graphical representations for a sample interferogram are shown in Figure 3.

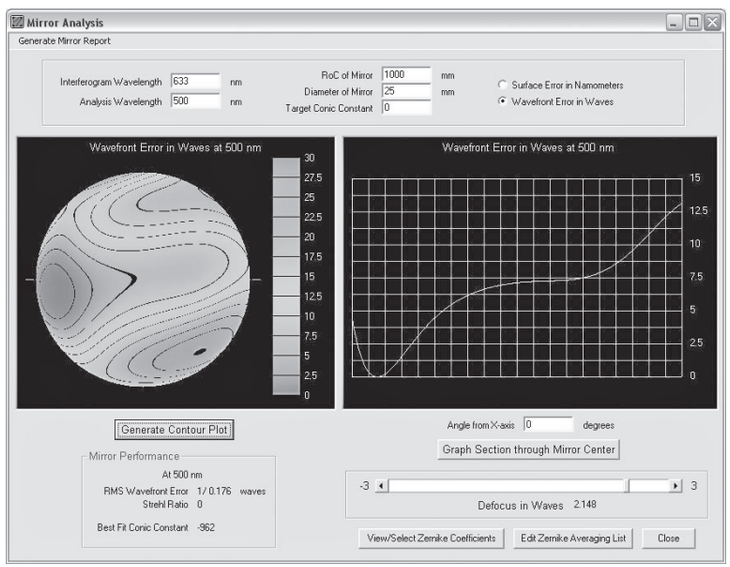

Figure 3: The Zernike coefficients are summed into contour and graphical displays in these panels.

The target conic section in the sample fit is a sphere and the mirror analysis was done at 500 nm. Because of the significant astigmatism, the PV aberration averages about 30 waves but is only about 10 waves along the best axis, with an rms aberration of about 10 waves for this 1 inch radius section. This result holds up for other areas measured across the mirror surface as well and we estimate, using the Holenstein, Mitchell, Koch (HMK) equation (23) from chapter 16 in this book, that the total waveform aberration for this surface is around 200 waves. Except for

gross edge defects such as wrinkles which should be masked off, one should expect less than 1000 waves rms aberration on a 1.6 meter mirror.

Reflectivity

The transmissions of unpressurized film samples were measured with beams from white photodiode and He-Ne laser sources with a precision of about ±2%. Film thinner than 2 mil was insufficiently metalized. Thicker film, on the other hand, showed essentially 0% transmission and this value remained stable for months. Reflectivities were much harder to measure. Diffuse reflection from microripple and microroughness of the film surface were probed by bouncing a laser beam off various spots on stretched, unpressurized film. As an example, a typical 5 mil sample showed a divergence due to diffuse reflection of 0.59(3) milliradian.

We have not checked the possibility that transmission and reflectivity change significantly when a pressure difference is applied to the film. This might happen because the metal domains themselves can become stretched and attenuated with a significant pressure difference.

Selected Imaging Results

Four of the mirror devices were made into skeletal telescopes with carbon fiber or aluminum structural members; one of these was intended to function as a broken-Cassegrain reflector, another worked as a prime-focus instrument and two as Newtonian telescopes. For the Newtonian configuration, the secondaries were aluminized glass flats while a pneumatic mirror with a positive pressure difference against atmospheric was used for the broken-Cassegrain. Only two of these instruments were attached to suitably stable mounts.

The newer 42 inch cell was loaded with the same 5 mil film for more than 6 months during which interval it had been pressure-cycled scores of times. By June, 2009 it was loose in its cell but was not re-tensioned before being taken outside where daytime ambient temperature was about 80° F. The appearance of the assembly is shown in the main part of Figure 4.

A pressure difference was established and the mirror aimed at a communications tower visible to the naked eye after being stabilized on an IPI393 tripod and GEM mount. The target was about 10,000 feet distant and was seen over the convection patterns from two intervening office parks of sunlit brick buildings and asphalt parking lots and a 4-lane highway at an elevation of about +5° above the mirror. A handheld digital camera made the image of the target shown as an insert in Figure 4 with the telescope working at approximately *f*/0.7. The resolution of the image is of the order of 10″.

Somewhat later, one of the 12 inch cells was loaded with 1 mil film and was mounted on an undriven optical table to obtain sample

images of bright stars. A column sum profile of a CCD image of Vega is shown in Figure 5. (Opposite)

Figure 4: A 42 inch cell and OTA mounted on an IPI393 GEM mount. A daytime image showing a near field of trees and a distant one of a structural tower is shown in the upper-right insert. The camera in automatic mode had difficulty deciding which fraction of the scene to focus on. The piecrust distortions around the edge of the image result from failing to re-tension the film in its cell. Stratified inversion layers above manmade structures account for the ragged tower image. In order to facilitate development testing, the inside cables on the truss members are not in place here and this condition caused the truss poles to bend inwards.

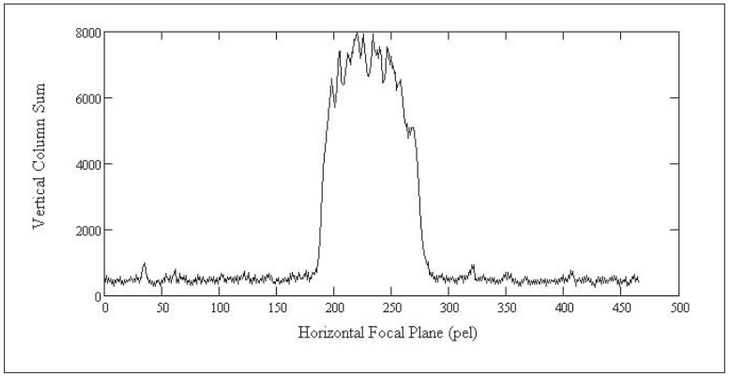

Figure 5: A CoC profile of Vega from a CCD image made with a 12 inch cell operating at *f*/4 using a factor of 0.5x focal reduction to *f*/2. The scale is 5.0 μm/pixel at the focal plane.

We find that a focal reducer lens placed prior to the prime focus of the telescope and in front of the detector markedly improves the character of the point spread function. The diameter of the CoC decreases by the focal reduction factor making the focal reducer act as a light concentrator. Also, some aberrations become less pronounced with the longer focal distances made possible by the use of the reducer, the dominant one being spherical aberration since it decreases as the cube of the focal ratio.

However, the diameter of the CoC encircling substantially all of the flux is about 0.5 mm in the figure. The prediction, using HMK equation (3), again from chapter 16 of this book, and the measurement of 200 rms waves aberration on the surface, is just 0.08 mm. The spherical aberration in this experiment was uncorrected and according to HMK equation (2) produces a spot 0.07 mm in diameter after the focal reducer. The local slope aberrations using HMK equations (15) and (17) with data from Table 1 amount to 0.32 mm. However, the interferogram sampled only a small area of the mirror and it is not clear (to the authors at least) that local slope aberrations in this case add in quadrature.

Co-added local slope aberrations, diffuse reflection from microripples, and non-random systemic surface defects are believed to be responsible for the discrepancy. The sample of 1 mil film used on Vega was not sampled for microripples, but the diffuse reflection of the 5 mil sample mentioned above would account for a 0.73 mm CoC. Understanding and diminishing this gap between prediction and experiment is an active area of research. Published vendor literature on commercial Mylar films indicate that microscopic particles are purposefully deposited on the film during manufacture to prevent the layers from sticking once the film is rolled. We expect that a solution to this problem may be found with vacuum aluminizing of low-surface-defect membrane materials.

Future

Figure 6 is a detail from a sketch for a 1.6 m mirror on an Alt-Az mount with control of the gross astigmatism of the primary mirror using push-pull screws placed on the mirror cell back and sides. If needed, secondary correction for significant Zernike coefficients may be done pseudo-statically or dynamically on a small deformable secondary feeding the detector. This design is expected to produce a CoC well under 1 mm. The mirror cell and tube assembly are expected to weigh less than 500 lbs and can be mounted on commercial off-the-shelf equatorial or Alt-Az mounts. The mirror cell may be made of cast aluminum with a vacuum-sealed epoxy finish to reduce costs and prevent air leakage. The entire structure is projected to cost under USD $65,000.

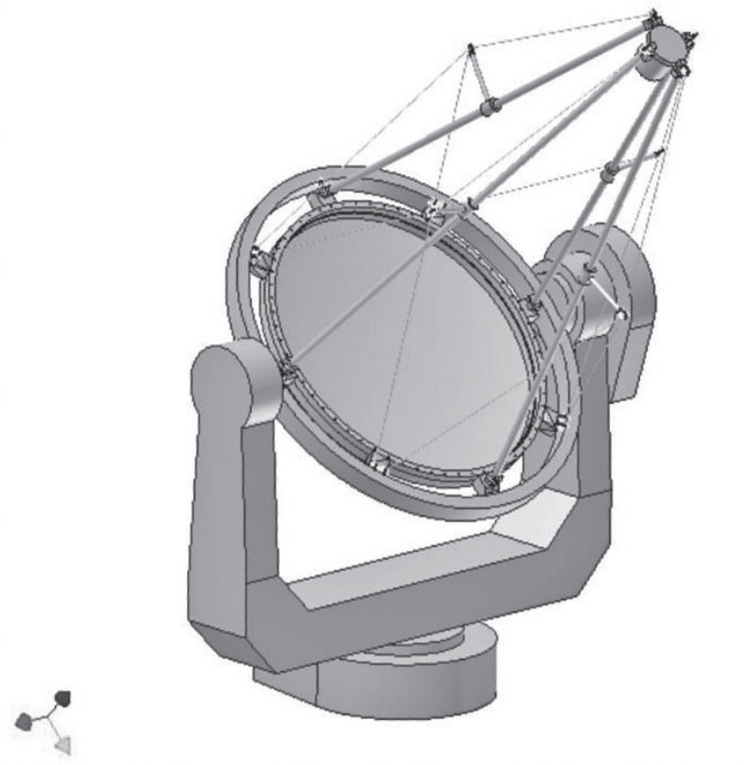

Figure 6: A sketch of one possible next-generation mounted trial mirror.

Conclusions

• We have been able to develop two varieties of cells that will maintain a pressure difference for the long term. Mylar permeability is not a problem. Bare Mylar against machined surfaces forms an airtight seal. There is no need to add rubber gasket or glue to hold the vacuum for hundreds of hours. Active air pressure stabilization is not needed for observing runs of less than an hour when the atmosphere is relatively stable. Fine focusing or vacuum adjustment is sufficient and can be automated if needed between observations.

• Edge clamping and pre-tensioning of Mylar can make wrinkle-free mirrors. Folding the Mylar before clamping causes wrinkles.

• Film thickness should be at least 4 mils for metalizing to be sufficiently reflective. Sources of aluminized film with low levels of microripple must be identified.

• Mirror cell and structural members should be made of metal. Wood and fiberglass were subject to flexure from the cycling of the modest air pressure differences needed to form a suitable surface and they suffered numerous leaks. For instance, a 3% atm pressure difference against atmospheric (commonly used by us) on the 42 inch cell (at *f*/2) results in about 600 lbs load on each of the cell rear and mirror faces.

• Membrane mirrors without astigmatism correction can produce figures with about 10 waves rms aberration peak-to-peak per inch. Our construction of a 1.6 m cell, however, is pending perfection of large-amplitude aberration control. This happens because rms aberrations of considerably less than 300 waves rms across the membrane surface, with rms gradient norms of just 4 waves, are needed in order to allow detectors to work adequately with 1 mm apertures. Our current plans for future research emphasize static and dynamic control of the primary mirror Zernike coefficients and secondary mirror waveform detection and control.

• We project that mirrors with large degrees of smooth aberrations may be used for astronomical research as light buckets in the not-too-distant future. Also, we expect that a pneumatic 1.6 m mirror cell and optical tube assembly, with adjustable figure control, will be transportable and be affordable for small research institutions. We project that the upper limit for pneumatic mirror telescopes will exceed 3 m using commercial films.

Authors' Note

Bruce D. Holenstein can be reached at Gravic, Inc., 301 Lindenwood Drive, Suite 100, Malvern, Pennsylvania 19355 USA.

References

Gavin, M. 1979. Aluminized mylar as a flux collector. *Sky and Telescope*, 57, 490.

Holenstein, B. D., Mitchell, R. J., and Koch, R. H. 2010. Light bucket mirror figures of merit. In *Lightweight Alt-Az Telescope Developments*, eds. Genet, R., Johnson, J., and Wallen, V. Santa Margarita, CA: Collins Foundation Press.

King, W., Waddell, P., and Raptodimos, T. 1985. Optics in engineering measurement. *Proc. of SPIE*, 599, 80.

Manly, Peter L. 1991. *Unusual Telescopes*, 15. Cambridge UK: Cambridge U. Press.

Rowe, David. 2003. FringeXP: A Fringe Analysis Program, Ver. 2. Available at http://www.ceravolo.com/fringeXP.html.